Available online at www.sciencedirect.com
SCIENCE DIRECT®
Composites Science and Technology 63 (2003) 1705–1722
COMPOSITES SCIENCE AND TECHNOLOGY
www.elsevier.com/locate/compscitech

Fiber waviness in nanotube-reinforced polymer composites—II: modeling via numerical approximation of the dilute strain concentration tensor

R.D. Bradshaw[1], F.T. Fisher, L.C. Brinson*

Department of Mechanical Engineering, Northwestern University, Evanston, IL 60208, USA

Received 30 September 2002; received in revised form 20 December 2002; accepted 10 January 2003

Abstract

Nanotube-reinforced polymers offer significant potential improvements over the pure polymer with regard to mechanical, electrical and thermal properties. This article investigates the degree to which the characteristic waviness of nanotubes embedded in polymers can impact the effective stiffness of these materials. A 3D finite element model of a single infinitely long sinusoidal fiber within an infinite matrix is used to numerically compute the dilute strain concentration tensor. A Mori–Tanaka model utilizes this tensor to predict the effective modulus of the material with aligned or randomly oriented inclusions. This hybrid finite element-micromechanical modeling technique is a powerful extension of general micromechanics modeling and can be applied to any composite microstructure containing non-ellipsoidal inclusions. The results demonstrate that nanotube waviness results in a reduction of the effective modulus of the composite relative to straight nanotube reinforcement. The degree of reduction is dependent on the ratio of the sinusoidal wavelength to the nanotube diameter. As this wavelength ratio increases, the effective stiffness of a composite with randomly oriented wavy nanotubes converges to the result obtained with straight nanotube inclusions. The approach developed in this paper can also be utilized in the analysis of other problems involving nanotube-reinforced polymers, including alternate nanotube representations, viscoelastic response, assessing the effect of low matrix-NT bond strength and in the determination of thermal and electrical conductivity.

Keywords: A. Nanostructures; A. PMCs; B. Mechanical properties; B. Modeling; C. FEA

1. Introduction and background

Composite materials offer the material designer the opportunity to combine two (or more) materials to optimize material properties. Many material properties and features can be modified, including stiffness, strength, toughness, durability, appearance, electrical behavior and thermal behavior. The proper choice and amount of the filler phase material is vital to achieving the desired properties. For applications where weight, stiffness and strength are critical, polymers reinforced with carbon nanotubes (NTs) offer the potential for significant improvement over systems such as graphite fiber reinforced polymers. For example, graphite fibers have modulus and strength values that range from 200 to 600 GPa and 2.5 to 6.5 GPa, respectively [1,2]. Carbon nanotubes are predicted to have modulus values on the order of 1 TPa, with strengths several times that of graphite fibers [3–8].

One area of current research interest is low volume fraction carbon nanotube-reinforced polymers (NRPs). Often the goal of creating such materials is to take advantage of the extraordinary electrical and thermal conductivity of NTs to create multifunctional NRPs with improved electrical and thermal properties [9]. Several investigators have demonstrated that such materials also have significant improvements in modulus and strength relative to the pure polymer matrix material [10–12]. However, the mechanical property enhancements which are currently realized with these materials are often significantly less than those suggested

* Corresponding author. Tel.: +1-847-2347; fax: +1-847-491-3915.
E-mail address: cbrinson@northwestern.edu (L.C. Brinson).
[1] Current address: Department of Mechanical Engineering, University of Louisville, Louisville, KY 40292, USA.

0266-3538/03/$ - see front matter © 2003 Elsevier Ltd. All rights reserved.
doi:10.1016/S0266-3538(03)00070-8

Nomenclature

a	Amplitude of sinusoidal NT
a/λ	Waviness ratio of sinusoidal NT
$\mathbf{A}^{r,\ \mathrm{dil}}$	Dilute strain concentration tensor/matrix for the rth phase
$\mathbf{A}$	Dilute strain concentration tensor/matrix for phase 1
$\hat{\mathbf{A}}$	Dilute strain concentration tensor/matrix from the Eshelby solution
$\mathbf{A}^{\mathrm{ALW}}$	Dilute strain concentration tensor/matrix from the analytical long wavelength model
$\mathbf{C}^r$	Modulus tensor/matrix for the rth phase
$\mathbf{C}^*$	Composite effective modulus tensor/matrix
d	Diameter of sinusoidal NT
E_{cell}	Young's modulus in NT direction for parallelepiped unit cell
E_{ERM}	Effective reinforcing modulus for single wavy NT
E_{M}	Modulus of matrix material (phase 0)
E_{NT}	Modulus of NT material (phase 1)
$E_{\mathrm{NT}}/E_{\mathrm{M}}$	Modulus ratio of sinusoidal NT
ERM	Effective Reinforcing Modulus (model)
f_{cell}	Volume fraction of NT in parallelepiped unit cell
f_r	Volume fraction for the rth phase
NT	Carbon nanotube
NRP	Nanotube-reinforced polymer
NSCT	Numerical Strain Concentration Tensor (model)
p	Constant used to define transformation matrix $\mathbf{T}(\alpha)$
$\mathbf{T}(\alpha)$	Transformation matrix for ALW model
u_i	Displacement function for specifying finite element model boundary conditions
v_q	Volume of qth NT element
V_1	Domain of NT (phase 1)
$\alpha(z)$	Angle between axis of NT segment and global z axis
$\tilde{\boldsymbol{\varepsilon}}$	Farfield applied strain
$\tilde{\boldsymbol{\varepsilon}}^{uvw}$	Farfield applied strain in local coordinate system of NT segment
$\tilde{\boldsymbol{\varepsilon}}^{123}$	Farfield applied strain in global coordinate system
$\boldsymbol{\varepsilon}^r$	Strain tensor function for the rth phase
$\langle\boldsymbol{\varepsilon}\rangle$	Average strain for the NRP composite
$\varepsilon_i^q\vert_{\tilde{\varepsilon}_p}$	Centroidal strain for qth NT element due to farfield applied strain $\tilde{\varepsilon}_p$
λ	Wavelength of sinusoidal NT
λ/d	Wavelength ratio of sinusoidal NT
ζ	Constant accounting for use of engineering shear strain
$\langle\ \rangle$	Volumetric averaging operation
$\{\}$	Orientational averaging operation
$\{\}_{\mathrm{TI}}$	Orientational averaging operation for randomization about the z axis
$\{\}_{\mathrm{3D}}$	Orientational averaging operation for randomization in all directions

by simple micromechanics models [13]. This may be caused by a variety of factors, including NT dispersion within the polymer, the nature of the interaction between the polymer and the NT, the size, shape and orientation of the NT, and the type of NT used (single wall, multi-wall, bundles, etc.).

One feature characteristic of NRPs is that the embedded NTs are not straight but rather have significant curvature or waviness that varies throughout the composite [11,14]. While it is reasonable to surmise that this waviness reduces the effectiveness of the NT reinforcement of the polymer, the degree to which this is the case is unclear. The goal of this work is to develop a micromechanics-based model that can be used to assess the effect of nanotube waviness on the properties of NRPs. The critical item that must be determined in such a micromechanics approach is the dilute strain concentration tensor, which for a single inclusion embedded in an infinite matrix material relates the average inclusion strain to the applied farfield strain. In a previous study [13] and in the companion article of this work [15], the problem was simplified by modeling the wavy NTs as infinitely long straight NTs; the effect of waviness was incorporated using a reduced effective nanotube modulus determined via finite element modeling. Since the wavy NT was modeled as a straight NT with a reduced modulus, the dilute strain concentration tensor could be determined analytically via Eshelby's solution for an ellipsoidal inclusion in an infinite matrix.

In the current work, an alternate approach is used. The NT is modeled as an infinitely long sinusoidal fiber and the dilute strain concentration tensor is obtained directly from a finite element solution. This approximates the NT and the surrounding matrix as a continuum; the nature of this assumption and its justification and limitations are discussed in the companion paper of this work [15][2] This Numerical Strain Concentration Tensor (NSCT) method is more complicated than the approach in the companion article, as six finite element solutions must be performed to determine

[2] Once the NT and surrounding matrix are modeled as a continuum, the length scale of the NT is no longer material to the analysis. Thus, the model developed in this article applies equally well to larger inclusions such as graphite fibers. As such, in this article the term fiber is used interchangeably with the term nanotube when speaking of the reinforcement phase of the composite material.

the 12 independent terms of the strain concentration tensor (versus 1 finite element solution to determine a single parameter in the companion article). However, this approach is more accurate and thus enables closer study of any composite with non-ellipsoidal inclusions. It will be shown that for an NRP with unidirectional wavy NTs, the predicted modulus in the NT direction is very similar for the two approaches. However, the modulus predicted in the plane of waviness in the direction normal to the NT axis is significantly higher in the current model, particularly as waviness increases. This difference impacts the prediction of the modulus of NRPs with randomly orientated inclusions; specifically, the current model predicts a higher NRP effective modulus than the model presented in the companion paper.

In addition to the finite element approach, an analytical method is presented which is applicable when the wavelength of a sinusoidal NT is long relative to its diameter. It is demonstrated that the finite element approach converges to this analytical solution as wavelength is increased. This analytical model has implications regarding the degree to which NT waviness reduces the effective reinforcement of NRPs.

1.1. Dilute strain concentration tensor

In this section, a brief outline of several underlying concepts used in standard micromechanical analysis is presented [16]. This description should provide a clear understanding of the use of the dilute strain concentration tensor in micromechanics. The numerical technique presented in this paper is geared towards determining this tensor for non-ellipsoidal inclusions (e.g. wavy nanotubes).

Consider a 2 phase composite consisting of a single, arbitrarily shaped inclusion (phase 1) perfectly bonded inside a matrix material (phase 0). For the purposes of this discussion, assume that the matrix is large enough to appear infinite to the inclusion and that this composite is initially in a stress-free state such that the stress at every point in the body is zero.[3] Under the application of a homogeneous strain $\tilde{\boldsymbol{\varepsilon}}$ at the matrix boundary, the volumetric average of the strain in phase 1 (the inclusion) is given by

$$\langle \boldsymbol{\varepsilon}^1 \rangle = \frac{\int_{V_1} \boldsymbol{\varepsilon}^1 \, \mathrm{d}V}{\int_{V_1} \mathrm{d}V} \tag{1}$$

where $\boldsymbol{\epsilon}^1$ and V_1 are the strain tensor function and domain of the inclusion, respectively, and the $\langle\ \rangle$ symbol denotes a volumetrically averaged quantity. If the matrix and inclusion are both linear elastic, and no separation occurs at their interface, there must be a linear relationship between the farfield strain tensor $\tilde{\boldsymbol{\varepsilon}}$ and the average inclusion strain tensor $\langle \tilde{\boldsymbol{\varepsilon}}^1 \rangle$. This relationship is expressed by the dilute strain concentration tensor $\mathbf{A}^{1,\,\mathrm{dil}}$ as

$$\langle \boldsymbol{\varepsilon}^1 \rangle = \mathbf{A}^{1,\mathrm{dil}} \tilde{\boldsymbol{\varepsilon}} \tag{2}$$

Suppose that the dilute strain concentration tensor $\mathbf{A}^{1,\,\mathrm{dil}}$ in Eq. (2) has been determined for a single inclusion of the type to be considered. For a 2 phase composite consisting of a number of identical inclusions, the effective elastic modulus tensor $\mathbf{C}^*$ can be determined. If the inclusions are well-dispersed and their volume fraction f_1 is small, the dilute approximation is employed and $\mathbf{C}^*$ is obtained algebraically as

$$\mathbf{C}^* = \mathbf{C}^0 + f_1 \left(\mathbf{C}^1 - \mathbf{C}^0\right) \mathbf{A}^{1,\mathrm{dil}} \tag{3}$$

where $\mathbf{C}^0$ and $\mathbf{C}^1$ are the elastic moduli of the matrix and inclusion phases, respectively.

As the inclusion volume fraction increases, interaction between the inclusions reduces the accuracy of the dilute approximation. In this case, the Mori–Tanaka theory provides an approach to determine the effective modulus $\mathbf{C}^*$ that includes the effect of particle interaction as

$$\mathbf{C}^* = \mathbf{C}^0 + f_1 \left(\mathbf{C}^1 - \mathbf{C}^0\right) \mathbf{A}^{1,\,\mathrm{dil}} \left[(1 - f_1)\,\mathbf{I} + f_1\,\mathbf{A}^{1,\,\mathrm{dil}}\right]^{-1} \tag{4}$$

where $\mathbf{I}$ is the identity tensor. Note that this expression yields the dilute approximation of Eq. (3) as the inclusion volume fraction f_1 approaches 0.

The Mori–Tanaka approach described in Eq. (4) provides a method for determining the elastic modulus of a 2 phase composite. It consists of a number of items that can be easily obtained ($\mathbf{C}^0$, $\mathbf{C}^1$, f_1) and one item that needs to be determined for the inclusion geometry under consideration ($\mathbf{A}^{1,\,\mathrm{dil}}$). In standard micromechanics, the Eshelby equivalent inclusion method is typically used to provide an analytical expression for $\mathbf{A}^{1,\,\mathrm{dil}}$ in the case of ellipsoidal inclusion shapes. The companion paper uses this approach and determines $\mathbf{A}^{1,\,\mathrm{dil}}$ by modeling the wavy nanotube as an infinitely long straight nanotube with an effective (reduced) modulus $\mathbf{C}^1$ obtained via

[3] The analysis performed in this article is based on small deformation linear elasticity. For this reason, the presence of residual stress/strain in the unloaded state (due to differential thermal expansion following cure, bending stress in the fibers due to configuration in the cured state, etc.) does not significantly affect the model developed in this article. In such a case, the effects of residual stress/strain are first determined in the absence of load. In the subsequent case when both load and residual stress/strain are present, the effect due to load alone is determined by subtracting the load-free result in an appropriate manner. The net result will be identical to that obtained by assuming an initially stress-free state; thus, the apparent modulus of such a material is not affected by the presence of residual strains. This approach does not apply to large deformation behavior that leads to fiber reorientation; models developed by other researchers can be used in such cases [17,18].

finite element analysis. In this paper, a method is developed to retain the NT shape and determine the strain concentration tensor $\mathbf{A}^{1,\ \mathrm{dil}}$ by evaluating the average nanotube strain as shown in Eq. (1) directly from a 3D finite element model. By solving a sufficient number of cases, $\mathbf{A}^{1,\ \mathrm{dil}}$ can be determined from the fundamental relationship provided in Eq. (2). This hybrid numerical-analytical micromechanics approach will be useful to help understand the properties and behavior of any multiphase material with non-ellipsoidal inclusions.

The expression contained in Eq. (4) is derived for inclusions with identical shape, properties and orientation (i.e. equivalent $\mathbf{A}^{1,\ \mathrm{dil}}$ in the global coordinate system). For NRPs, however, the nanotubes are typically oriented in random directions. There are several approaches that can be used to analyze such materials [19,20]. This paper will use the Mori–Tanaka approach presented by Weng [21], which demonstrated that an N phase composite with variably oriented inclusions has an effective modulus $\mathbf{C}^*$ given by

$$\mathbf{C}^* = \left[\sum_{r=0}^{N-1} f_r \left\{\mathbf{C}^r\,\mathbf{A}^{r,\ \mathrm{dil}}\right\}\right]\left[\sum_{r=0}^{N-1} f_r \left\{\mathbf{A}^{r,\ \mathrm{dil}}\right\}\right]^{-1} \tag{5}$$

where f_r, $\mathbf{C}^r$ and $\mathbf{A}^{r,\ \mathrm{dil}}$ are the volume fraction, modulus tensor and dilute strain concentration tensor for the rth phase, respectively, and operation $\{\mathbf{X}\}$ designates the orientational average of tensor $\mathbf{X}$, discussed in more detail in a later section.[4] Any distribution of inclusion orientations can be considered by specifying the appropriate {} form. Two common orientational operations are randomness in a single plane (2D random composite) or randomness in all directions (3D random composite). The case of identically aligned inclusions [as in Eq. (4)] corresponds to $\{\mathbf{X}\} = \mathbf{X}$. Thus, the effective elastic properties for an NRP with N phases of wavy randomly oriented nanotubes can be easily obtained once the dilute strain concentration tensor $\mathbf{A}^{r,\ \mathrm{dil}}$ has been determined for each inclusion phase using the approach described below. In this paper, NRPs with 2 phases are studied (i.e. $N=2$), consisting of a single type of nanotube inclusion ($r=1$) embedded in a matrix phase ($r=0$); see the companion article for an analysis of an NRP consisting of several nanotube inclusion phases (i.e. $N > 2$) [15].

2. Finite element model

As described in the previous section, the item to be determined for a micromechanical analysis of the modulus of an NRP with wavy NTs is the strain concentration tensor $\mathbf{A}^{1,\ \mathrm{dil}}$. This article develops a new method, called the Numerical Strain Concentration Tensor (NSCT) model, to determine $\mathbf{A}^{1,\ \mathrm{dil}}$ for a non-ellipsoidal inclusion using a finite element model. This section will describe the geometry, mesh, boundary conditions and solution of the finite element model. This section will also describe how a slightly modified model is used to determine the key parameter for the Effective Reinforcing Modulus (ERM) model developed in the companion paper. Analysis of NRPs with aligned and randomly oriented wavy NTs utilizing the finite element results will be described in a subsequent section.

2.1. Assumed wavy fiber characteristics

In an NRP composite, the NTs exhibit a great deal of variation, including the length of individual NTs relative to their diameter, the shape of the embedded NTs, and their orientation relative to one another. In order to perform a finite element analysis of an NRP with wavy NTs, simplifications of the geometry must be made to reduce the problem to one that can be computationally solved in a reasonable time frame.

For this article, a single wavy NT of diameter d embedded in a nearly-infinite matrix is analyzed. It is assumed that the NT has a solid cross-section, is infinitely long and its centerline path is sinusoidal in the y–z plane at $x=0$ and is given by

$$y = a\cos\left(\frac{2\pi z}{\lambda}\right) \tag{6}$$

where a and λ are the amplitude and wavelength of the NT waviness, respectively. In the stress-free state, the NT cross-section in all planes normal to the centerline path given in Eq. (6) is a circle with diameter d equal to the NT diameter. This representation of the NT is particularly useful as it introduces planes of symmetry at $x=0$ and $z = n\,\lambda\,/\,2$, where n is an integer.

This geometry can be analyzed by a fairly compact finite element model. This leads to a reasonable solution time, which permits consideration of a number of variables. However, this approach also limits the types of cases that can be considered. For example, NTs generally do not follow regular sinusoidal paths as approximated here. Furthermore, although NTs are typically long relative to their diameter (often on the order of 10^3–10^4 d), they are clearly not infinite in length; the effect of NT termination is not considered in this model. Also, NTs are not solid but hollow; the impact of using a hollow NT representation in the finite element model has not yet been evaluated. Thus, this work should be viewed as a beginning in the analysis of NRPs with wavy NTs that will give a good first

[4] Since the dilute case considers a single inclusion in an infinite matrix, the average matrix strain is identical to the applied farfield strain; thus, the dilute strain concentration tensor for the matrix, $\mathbf{A}^{0,\ \mathrm{dil}}$, is the identity tensor.

approximation of the effective modulus. Future efforts will be aimed at addressing other important issues, such as the effect of finite NT length, hollow NT configurations, or alternate NT paths on effective reinforcement. An ideal model would permit predictions for a single NT with an arbitrary path embedded in a matrix.

2.2. Finite element model mesh

The finite element analysis in this article is performed using ANSYS™. Two types of models are used in the analysis for this article and the companion paper; these are shown in Fig. 1. For the analysis that determines the strain concentration matrix, the shape of the matrix boundary is irrelevant; the model in Fig. 1(a) is used in this case. For the effective reinforcing modulus approach in the companion paper, the model needs to be a parallelepiped in order to calculate the effective modulus of the model in the z direction; the model in Fig. 1(b) is used in this case. Fig. 1(c) shows a close-up of the elements that makeup the NT and the adjacent matrix. For clarity, the models shown have fairly high NT volume fractions (on the order of 0.5%); the models used for actual analysis have volume fractions on the order of 0.01% to ensure that the matrix appears infinitely large to the NT.

The model is built from a series of 4 sided areas constructed at various points along the fiber path; those that make up the fiber are constructed normal to the fiber path while those that remain are either normal to the global z axis or skewed as necessary. The volumes of the model are then constructed by connecting these area sets with a series of lines and arcs; arcs are used for the NT volumes to reflect the curved surfaces of the NT while straight lines are used for the remainder. The volumes comprising the NT and matrix immediately adjacent to it are meshed using 20 node bricks containing midside nodes. This allows element edges to be parabolic in shape, which accurately captures the curved NT surface. These higher order elements are also well suited to modeling the high strain gradients that exist close to the NT. The remaining volumes are meshed with 8 node bricks to reduce the number of degrees freedom while still providing sufficient detail to capture the slowly varying strain fields closer to the model exterior. The resulting model is quarter-symmetric; mirroring this model about $x=0$ and then $z=0$ will create a model of a single wavelength λ of a sinusoidal NT embedded in an apparently infinite matrix material.

2.3. Boundary conditions—strain concentration matrix determination

In order to determine the strain concentration matrix $\mathbf{A}^{1,\,\mathrm{dil}}$, six strain cases need to be applied to the model. These consist of the three farfield extensional strains ($\tilde{\varepsilon}_{11}$, $\tilde{\varepsilon}_{22}$, $\tilde{\varepsilon}_{33}$) and the three farfield shear strains ($\tilde{\varepsilon}_{23}$, $\tilde{\varepsilon}_{13}$,

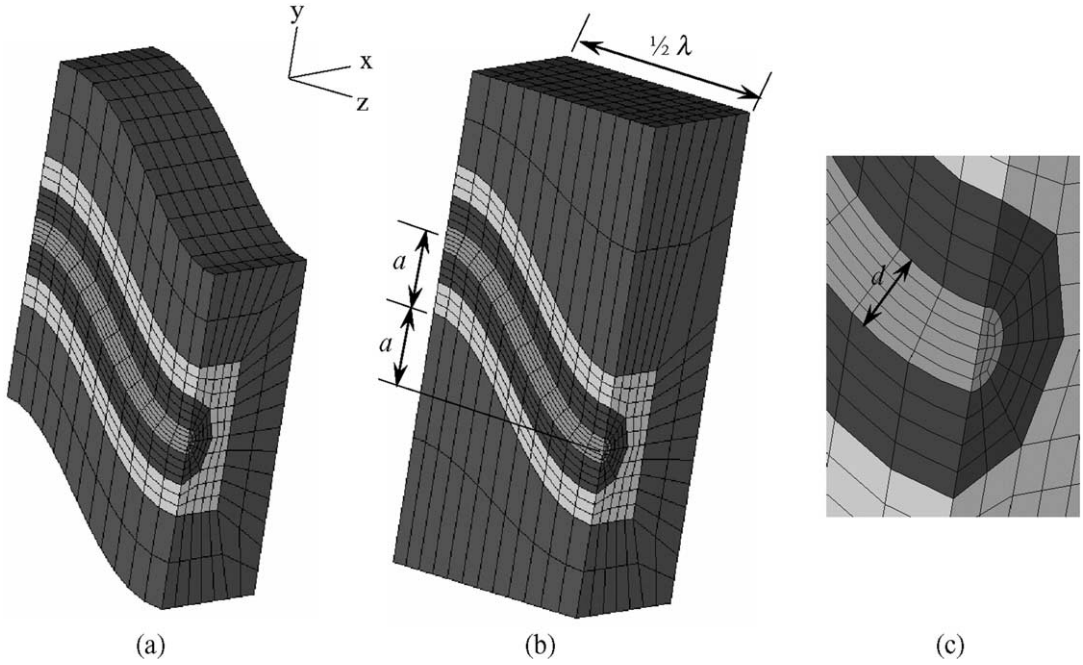

Fig. 1. Examples of finite element models used in the analysis: (a) wavy matrix boundary; (b) parallelepiped matrix boundary; (c) close-up of elements that makeup NT and adjacent matrix; shading represents NT and three distinct matrix regions (representative xyz coordinate system and geometry terms a, λ and d also shown).

$\tilde{\varepsilon}_{12}$).[5] For each case, one strain condition is applied to the model while all other strains are specified to be 0. An additional complication is that the quarter-symmetric model consists of a number of symmetry (and anti-symmetry) planes that must be accounted for appropriately. To clarify the definitions, Fig. 2 shows the surfaces for which boundary conditions must be specified. Plane 4 and surfaces 2 and 5 are model exteriors while planes 1, 3 and 6 are model interior planes of symmetry.

The strains on the model exteriors are applied by specifying the displacements at every node. The nodal displacements **u** are obtained based upon the position of the node in the global coordinate system as

$$u_1 = f(x, y, z) \quad ; \quad u_2 = g(x, y, z) \quad ; \quad u_3 = h(x, y, z) \tag{7}$$

These displacement functions are given in Table 1. By inspection, these displacements cause the desired farfield strain in each row of Table 1 while causing all other strains to be 0 in accordance with the tensorial strain relationship

$$\varepsilon_{ij} = \frac{1}{2}\left(u_{i,j} + u_{j,i}\right) \tag{8}$$

The model interior planes are somewhat more complicated. Each plane represents a plane of symmetry:

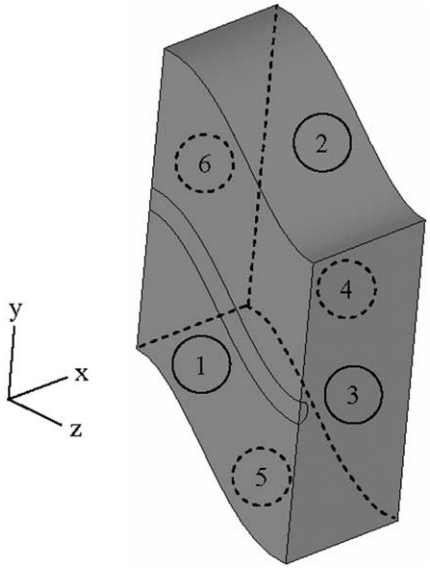

Fig. 2. Numbered planes and surfaces used for strain boundary conditions (solid circles indicate visible planes, dashed circles indicate planes hidden in the view).

[5] The boundary conditions are specified using tensorial shear strains, which are indicated with an ϵ. Later in the paper, engineering shear strains will be used to be consistent with previous work; these are indicated by a γ.

mirroring about plane 1 and then either plane 3 or plane 6 creates an entire cell representing a single wavelength λ of the sinusoidal NT. This captures the infinitely long nature of the sinusoidal NT since the geometry repeats with offsets of $n\ \lambda$ in the z direction, where n is an integer. However, it will be demonstrated that the quarter-symmetric model shown in Fig. 1 is sufficient to capture the behavior. Three types of symmetry are required to specify the boundary conditions on the 3 symmetry planes for the 6 strain cases:

- Symmetry: displacement normal to plane is fixed at zero and the nodes are free to displace in the plane
- Anti-symmetry: displacements in the plane are fixed at zero and the nodes are free to displace normal to the plane
- Modified Symmetry: displacement normal to plane is fixed at a non-zero value and the nodes are free to displace in the plane

The displacement conditions for these planes are listed in Table 2. For each case, visualization of the displacements can be used to demonstrate the validity of the specified boundary conditions. These conditions were also validated by demonstrating the results from a quarter-symmetric model (as above) were identical to those from the solution of a full model (mirrored about planes 1 and 6); this result will be discussed in the next section.

Table 1
Displacement functions for exterior model surfaces (plane 4 and surfaces 2 and 5 in Fig. 2)

	Displacement $u_1 f(x, y, z)$	Displacement $u_2 g(x, y, z)$	Displacement $u_3 h(x, y, z)$
Farfield strain $\tilde{\varepsilon}_{11}$	$\tilde{\varepsilon}_{11}\ x$	0	0
Farfield strain $\tilde{\varepsilon}_{22}$	0	$\tilde{\varepsilon}_{22}\ y$	0
Farfield strain $\tilde{\varepsilon}_{33}$	0	0	$\tilde{\varepsilon}_{33}\ z$
Farfield strain $\tilde{\varepsilon}_{23}$	0	0	$2\ \tilde{\varepsilon}_{23}\ y$
Farfield strain $\tilde{\varepsilon}_{13}$	0	0	$2\ \tilde{\varepsilon}_{13}\ x$
Farfield strain $\tilde{\varepsilon}_{12}$	$\tilde{\varepsilon}_{12}\ y$	$\tilde{\varepsilon}_{12}\ x$	0

Table 2
Specified displacements for interior model surfaces (displacements not specified are free) (S) = symmetry, (M) = modified symmetry, (A) = anti-symmetry

	Plane 1 $x = 0$	Plane 3 $z = \lambda\ /\ 2$	Plane 6 $z = 0$
Farfield strain $\tilde{\varepsilon}_{11}$	$u_1 = 0$ (S)	$u_3 = 0$ (S)	$u_3 = 0$ (S)
Farfield strain $\tilde{\varepsilon}_{22}$	$u_1 = 0$ (S)	$u_3 = 0$ (S)	$u_3 = 0$ (S)
Farfield strain $\tilde{\varepsilon}_{33}$	$u_1 = 0$ (S)	$u_3 = 1/2\ \tilde{\varepsilon}_{33}\ \lambda$ (M)	$u_3 = 0$ (S)
Farfield strain $\tilde{\varepsilon}_{23}$	$u_1 = 0$ (S)	$u_1 = u_2 = 0$ (A)	$u_1 = u_2 = 0$ (A)
Farfield strain $\tilde{\varepsilon}_{13}$	$u_2 = u_3 = 0$ (A)	$u_1 = u_2 = 0$ (A)	$u_1 = u_2 = 0$ (A)
Farfield strain $\tilde{\varepsilon}_{12}$	$u_2 = u_3 = 0$ (A)	$u_3 = 0$ (S)	$u_3 = 0$ (S)

2.4. Solution for strain concentration matrix

Once the boundary conditions are applied for any of the six strain cases to be considered, ANSYS is used to determine the solution and perform all post-processing. The goal is to determine the relationship between the average NT strain and the farfield applied strain. Before proceeding, it is useful to simplify the strain concentration tensor from the $A^{1,\,\mathrm{dil}}_{ijkl}$ notation of Eq. (2) to a more compact 6×6 matrix form defined as

$$\langle \varepsilon_i^1 \rangle = A_{ij}\,\tilde{\varepsilon}_j$$

$$\begin{Bmatrix} \langle \varepsilon_{11}^1 \rangle \\ \langle \varepsilon_{22}^1 \rangle \\ \langle \varepsilon_{33}^1 \rangle \\ \langle \varepsilon_{23}^1 \rangle \\ \langle \varepsilon_{13}^1 \rangle \\ \langle \varepsilon_{12}^1 \rangle \end{Bmatrix} = \begin{bmatrix} A_{11} & A_{12} & A_{13} & A_{14} & A_{15} & A_{16} \\ A_{21} & A_{22} & A_{23} & A_{24} & A_{25} & A_{26} \\ A_{31} & A_{32} & A_{33} & A_{34} & A_{35} & A_{36} \\ A_{41} & A_{42} & A_{43} & A_{44} & A_{45} & A_{46} \\ A_{51} & A_{52} & A_{53} & A_{54} & A_{55} & A_{56} \\ A_{61} & A_{62} & A_{63} & A_{64} & A_{65} & A_{66} \end{bmatrix} \begin{Bmatrix} \tilde{\varepsilon}_{11} \\ \tilde{\varepsilon}_{22} \\ \tilde{\varepsilon}_{33} \\ \tilde{\varepsilon}_{23} \\ \tilde{\varepsilon}_{13} \\ \tilde{\varepsilon}_{12} \end{Bmatrix} \tag{9}$$

For the remainder of the paper, the $^{1,\mathrm{dil}}$ superscript is discarded for simplicity; it is implied that A_{ij} refers to the dilute strain concentration matrix for the NT (phase 1).

Suppose that one of the farfield strain conditions $\tilde{\varepsilon}_p$ ($p \in [1,\ 6]$) from Tables 1 and 2 are applied to the finite element model. After model solution, the volumetrically averaged strain $\langle \varepsilon_i^1 \rangle|_{\tilde{\varepsilon}_p}$ in the Q elements that make up the NT is given as

$$\langle \varepsilon_i^1 \rangle|_{\tilde{\varepsilon}_p} = \frac{\int_{V_1} \varepsilon_i^1|_{\tilde{\varepsilon}_p}\,\mathrm{d}V}{\int_{V_1} \mathrm{d}V} \approx \frac{\sum_{q=1}^{Q} \widehat{\varepsilon_i^q}|_{\tilde{\varepsilon}_p}\, v_q}{\sum_{q=1}^{Q} v_q} \quad ; \quad i \in [1,\ 6] \tag{10}$$

where v_q and $\varepsilon_i^q|_{\tilde{\varepsilon}_p}$ are the element volume and ith strain component at the element centroid, respectively, for the qth element that makes up the NT. Combining Eq. (9), evaluated for the single non-zero farfield strain $\tilde{\varepsilon}_p$, with the average fiber strains from Eq. (10) allows 6 of the 36 strain concentration matrix terms to be evaluated as

$$A_{ip} = \frac{\langle \varepsilon_i^1 \rangle|_{\tilde{\varepsilon}_p}}{\tilde{\varepsilon}_p} \quad (p \in [1,\ 6]) \tag{11}$$

This approach is repeated for all 6 components of farfield strain and the strain concentration matrix is fully determined.

The strain concentration matrix was determined via Eqs. (10) and (11) using a quarter-symmetric model (see Fig. 2) with a variety of sinusoidal geometries and material properties. The resulting strain concentration matrix for the quarter-symmetric model has the form

$$\mathbf{A} = \begin{bmatrix} A_{11} & A_{12} & A_{13} & A_{14} & 0 & 0 \\ A_{21} & A_{22} & A_{23} & A_{24} & 0 & 0 \\ A_{31} & A_{32} & A_{33} & A_{34} & 0 & 0 \\ A_{41} & A_{42} & A_{43} & A_{44} & 0 & 0 \\ 0 & 0 & 0 & 0 & A_{55} & A_{56} \\ 0 & 0 & 0 & 0 & A_{65} & A_{66} \end{bmatrix} \tag{12}$$

In order to verify the correctness of the boundary conditions on the planes of symmetry, the strain concentration matrix was also determined using a full model (created by mirroring the quarter-symmetric model in Fig. 2 about plane 1 and then about plane 6). The resulting strain concentration matrix is numerically identical to that shown in Eq. (12) with the exception that the full model finds the terms A_{14}, A_{24}, A_{34}, A_{41}, A_{42}, A_{43}, A_{56} and A_{65} to be zero. Consideration of the symmetry involved in the problem indicates the reason for this finding. Specifically, the sign of various shear strain terms changes in the four quadrants that make up the full model, causing the average NT shear strains to cancel. By only considering one-quarter of the full model, these associated terms do not cancel. This oversight can be corrected by bookkeeping, and the strain concentration matrix is determined from the quarter-symmetric model with the terms A_{14}, A_{24}, A_{34}, A_{41}, A_{42}, A_{43}, A_{56} and A_{65} discarded. With this, the final form of the strain concentration matrix[6] becomes

$$\mathbf{A} = \begin{bmatrix} A_{11} & A_{12} & A_{13} & 0 & 0 & 0 \\ A_{21} & A_{22} & A_{23} & 0 & 0 & 0 \\ A_{31} & A_{32} & A_{33} & 0 & 0 & 0 \\ 0 & 0 & 0 & A_{44} & 0 & 0 \\ 0 & 0 & 0 & 0 & A_{55} & 0 \\ 0 & 0 & 0 & 0 & 0 & A_{66} \end{bmatrix} \tag{13}$$

The finite element modeling technique described above produces the dilute strain concentration tensor for an infinitely long sinusoidal NT embedded in an infinite matrix. This approach can also be used to obtain the dilute strain concentration tensor for other inclusion types. Once a finite element model is created and solved with appropriate boundary conditions for the inclusion type to be considered, the average inclusion strain is analyzed via Eqs. (10) and (11) which again leads to the associated dilute strain concentration tensor. Thus, the approach described in this paper can be used in the study of any multiphase composite consisting of non-ellipsoidal inclusions.

[6] It should be noted that there is no coupling of shear and extension strains in Eq. (13). Thus, this strain concentration matrix can be used to relate farfield and average NT strain vectors consisting of either tensorial shear strains (ε_{23}, ε_{13}, ε_{12}) or engineering shear strains ($\gamma_{23} = 2\varepsilon_{23}$, $\gamma_{13} = 2\varepsilon_{13}$, $\gamma_{12} = 2\varepsilon_{12}$).

2.5. Boundary conditions and solution—effective reinforcing modulus

The companion article to this work uses a similar finite element procedure to determine an effective reinforcing modulus for the NT that accounts for NT waviness. This is accomplished by first determining the effective modulus of the parallelepiped cell containing the wavy NT (E_{cell}) as shown in shown in Fig. 1(b). This case is analogous to a unidirectional tension test in the z direction. Since the problem is symmetric about planes 3 and 6, the strain ε_{33} is constant at all points in those planes. Denoting the value of this strain as ε_{33}^0, the boundary conditions for the model interior planes are identical to those in Table 2 for the $\tilde{\varepsilon}_{33}$ case. The model exterior surfaces (planes 2, 4 and 5) are left traction free (no displacements specified). Such a model is unrestrained in the y direction; to prevent rigid body motion, a single (arbitrary) point is specified to have $u_2 = 0$.

To solve for the effective modulus of the cell, the total force F_z required to cause the strain $\tilde{\varepsilon}_{33}$ is calculated by summing the forces in the z direction applied to the nodes that make up Plane 3 (or, equivalently, Plane 6). The cell modulus E_{cell} is then simply calculated by dividing the average stress by the average strain as

$$E_{\text{cell}} = \frac{F_z}{A_{\text{Plane 3}}} \frac{1}{\varepsilon_{33}^0} \tag{14}$$

where $A_{\text{Plane 3}}$ is the area of Plane 3. The relationship to determine the effective reinforcing modulus E_{ERM} from E_{cell} is described in the companion paper as

$$E_{\text{ERM}} = \frac{E_{\text{cell}} - (1 - f_{\text{cell}})E_{\text{M}}}{f_{\text{cell}}} \tag{15}$$

where f_{cell} is the volume fraction of the NT in the unit cell.

2.6. Finite element model validation

In order to verify the accuracy of the preceding sections, a number of validation studies were performed. These ensure that the given boundary conditions are correct, that the matrix used is sufficiently large to approximate infinite matrix conditions and that the number of elements used in a given cross-section and in the direction of the NT are sufficient to achieve stable, accurate results. These conditions are satisfied for the models used in the remainder of this paper. Additional details are available elsewhere [22]

3. Models for NRP modulus

The numerical approach in the previous section is used to determine the dilute strain concentration matrix, **A**, for a sinusoidally shaped NT. Once **A** is obtained, traditional micromechanics techniques are employed to find the effective properties of composites with non-dilute volume fractions of sinusoidal inclusions. In this section, the Mori–Tanaka theory is used to determine the effective modulus for two NRP composites: the first has similarly oriented sinusoidal inclusions (Fig. 3a) while the second has sinusoidal inclusions randomly oriented in all directions (Fig. 3b); this development follows the approach of Weng [21] The combination of the numerically derived **A** and the Mori–Tanaka theory is referred to as the NSCT (numerical strain concentration tensor) model. An analytical solution is also developed for the limit case of long wavelength fibers, which is useful for model validation. This work is motivated by the need to understand and model the effects of carbon nanotubes in polymer composites; as such, all examples and

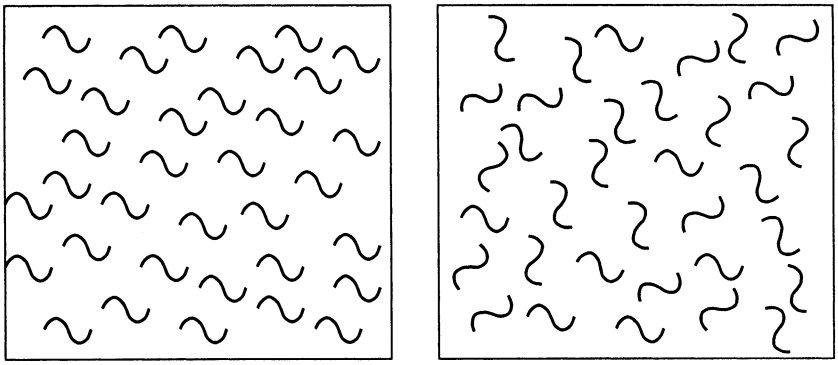

Fig. 3. Wavy NT orientations modeled: (a) similarly oriented wavy NTs with common axis directions and waviness planes; (b) wavy NTs randomly oriented in all directions with randomly oriented planes of waviness.

results are limited to these materials. However, this hybrid numerical-analytical micromechanics method is valid for any composite containing non-ellipsoidal inclusions.

3.1. Governing parameters

The finite element model in the previous section provides the ability to calculate either the strain concentration matrix **A** or the effective reinforcing modulus E_{ERM} for a single infinitely long sinusoidal NT embedded in an apparently infinite matrix. In addition to the mesh details described in the previous section, there are seven geometry and property values that must be specified: (1) the NT diameter d; (2) the sinusoidal wavelength λ; (3) the sinusoidal amplitude a; (4) the NT modulus E_{NT}; (5) the NT Poisson's ratio ν_{NT}; (6) the matrix modulus E_{M}, (7) the matrix Poisson's ratio ν_{M}. This assumes that both the NT and the matrix are isotropic materials; other material models could be used as well with the associated additional material parameters.

As described in the companion article, a dimensional analysis demonstrates that only 5 of these values are actually independent, with one dependent length term and one dependent stress term. As discussed in the companion paper, the Poisson's ratios for both phases are assumed to be 0.30 for all cases in this article; this reduces the variable count while remaining representative for structural polymers and consistent with NT experimental findings [5,6]. Furthermore, the companion article demonstrated that the effective reinforcing modulus is fairly insensitive to either ν_{NT} or ν_{M}; thus, a typical value is chosen to simplify the analysis. This reduces the number of variables to three, which for this study are chosen to be the wavelength ratio λ/d, the waviness ratio a/λ and the modulus ratio $E_{\mathrm{NT}}/E_{\mathrm{M}}$. Since the focus of this article is on polymers reinforced with NTs, the modulus ratio will be limited to two fairly large values of 200 and 400. Assuming a fairly typical polymer modulus of 2.5 GPa, these values correspond to a NT moduli of 500 and 1000 GPa.

3.2. Modulus of NRP with Similarly Oriented Wavy NTs

The effective modulus $\mathbf{C}^*$ for a 2 phase unidirectional NRP consisting of similarly oriented wavy NTs (Fig. 3a) with identical properties (λ/d, a/λ, $E_{\mathrm{NT}}/E_{\mathrm{M}}$) can be determined using Eq. (5) with the orientational operation $\{\mathbf{X}\} = \mathbf{X}$. The only unknown in this equation, $\mathbf{A}\left(=\mathbf{A}^{1,dil}\right)$, is first determined using the finite element method previously described. The effective modulus $\mathbf{C}^*$ can also be written in contracted 6×6 form [23] as

$$\langle\sigma_i\rangle = C^*_{ij}\langle\varepsilon_j\rangle$$

$$\begin{Bmatrix}\langle\sigma_{11}\rangle\\ \langle\sigma_{22}\rangle\\ \langle\sigma_{33}\rangle\\ \langle\sigma_{23}\rangle\\ \langle\sigma_{13}\rangle\\ \langle\sigma_{12}\rangle\end{Bmatrix} = \begin{bmatrix} C^*_{1111} & C^*_{1122} & C^*_{1133} & 0 & 0 & 0\\ C^*_{1122} & C^*_{2222} & C^*_{2233} & 0 & 0 & 0\\ C^*_{1133} & C^*_{2233} & C^*_{3333} & 0 & 0 & 0\\ 0 & 0 & 0 & C^*_{2323} & 0 & 0\\ 0 & 0 & 0 & 0 & C^*_{1313} & 0\\ 0 & 0 & 0 & 0 & 0 & C^*_{1212}\end{bmatrix} \begin{Bmatrix}\langle\varepsilon_{11}\rangle\\ \langle\varepsilon_{22}\rangle\\ \langle\varepsilon_{33}\rangle\\ \langle 2\,\varepsilon_{23}\rangle\\ \langle 2\,\varepsilon_{13}\rangle\\ \langle 2\,\varepsilon_{12}\rangle\end{Bmatrix} \tag{16}$$

Once the modulus of the individual phases ($\mathbf{C}^r$) are cast in 6×6 form, Eq. (5) is used to determine $\mathbf{C}^*$. The resulting material will be orthotropic as expressed in Eq. (16).

3.3. Modulus of NRP with randomly oriented wavy NTs

The preceding section determined the effective modulus $\mathbf{C}^*$ for a unidirectional NRP. However, typical NRPs have NTs randomly oriented in the matrix (Fig. 3b). The effective modulus for a 2 phase composite consisting of NTs with common values of λ/d, a/λ and $E_{\mathrm{NT}}/E_{\mathrm{M}}$ but randomly oriented in all directions in a matrix can also be determined using Weng's approach as presented in Eq. (5) [21]. The strain concentration matrix **A** is determined as in the unidirectional case. The orientational operation for 3D randomization is most easily envisioned in two steps. In the first, the {} operation accounts for a random rotation of the NT about its z axis; when performed on the matrix **X**, this operation, denoted $\{\}_{\mathrm{TI}}$, results in the transversely isotropic matrix $\mathbf{X}^{\mathrm{TI}}$ given by[7]

$$\begin{aligned}
&\mathbf{X}^{\mathrm{TI}} = \{\mathbf{X}\}_{\mathrm{TI}}\\
&X^{\mathrm{TI}}_{11} = X^{\mathrm{TI}}_{22} = \frac{3X_{11} + X_{12} + X_{21} + 3X_{22} + 2\,\zeta\,X_{66}}{8}\\
&X^{\mathrm{TI}}_{33} = X_{33} \quad ; \quad X^{\mathrm{TI}}_{44} = X^{\mathrm{TI}}_{55} = \frac{X_{44} + X_{55}}{2}\\
&X^{\mathrm{TI}}_{66} = \frac{X_{11} - X_{12} - X_{21} + X_{22} + 2\,\zeta\,X_{66}}{4\,\zeta}\\
&X^{\mathrm{TI}}_{12} = X^{\mathrm{TI}}_{21} = \frac{X_{11} + 3X_{12} + 3X_{21} + X_{22} - 2\,\zeta\,X_{66}}{8}\\
&X^{\mathrm{TI}}_{13} = X^{\mathrm{TI}}_{23} = \frac{X_{13} + X_{23}}{2} \quad ; \quad X^{\mathrm{TI}}_{31} = X^{\mathrm{TI}}_{32} = \frac{X_{31} + X_{32}}{2}
\end{aligned} \tag{17}$$

[7] The orientational average of a fourth-order tensor is given by $\{X_{ijkl}\} = \frac{1}{\alpha}\int_{\Omega} a_{ip}a_{jq}a_{kr}a_{is}X_{pqrs}d\Omega$ where Ω represents the orientational space, $\boldsymbol{a}$ is the appropriate transformation matrix relating local to global coordinates, X_{pqrs} is the fourth-order tensor in the local coordinate system, $\{X_{ijkl}\}$ is the resulting orientational average in the global coordinate system and α is an integration factor. In the cases given, the fourth order tensor was subsequently converted to 6×6 matrix form.

where ζ accounts for the use of engineering shear strains in the matrix definitions associated with Eq. (5): for $\mathbf{X} = \mathbf{C}^r\mathbf{A}^{r,\,\mathrm{dil}}$, $\zeta = 1$; for $\mathbf{X} = \mathbf{A}^{r,\,\mathrm{dil}}$, $\zeta = 2$. For NRPs with wavy NTs randomly oriented in all directions, these matrices must then be randomized using the $\{\}_{3D}$ operation given by

$$\begin{aligned}
\mathbf{X}^{3D} &= \left\{\mathbf{X}^{TI}\right\}_{3D} = \left\{\{\mathbf{X}\}_{TI}\right\}_{3D} \\
X_{11}^{3D} &= X_{22}^{3D} = X_{33}^{3D} = \frac{8X_{11} + 2X_{13} + 2X_{31} + 3X_{33} + 4\zeta X_{44}}{15} \\
X_{12}^{3D} &= X_{21}^{3D} = X_{13}^{3D} = X_{31}^{3D} = X_{23}^{3D} = X_{32}^{3D} \\
&= \frac{X_{11} + 5X_{12} + 4X_{13} + 4X_{31} + X_{33} - 2\zeta X_{44}}{15} \\
X_{44}^{3D} &= X_{55}^{3D} = X_{66}^{3D} = \frac{X_{11}^{3D} - X_{12}^{3D}}{\zeta}
\end{aligned} \tag{18}$$

The resulting isotropic matrices are then used to determine the effective modulus $\mathbf{C}^*$ for an NRP with 3D randomly aligned inclusions via Eq. (5). Note that in the companion paper, the randomization about the z axis provided by $\{\}_{TI}$ is not necessary since the inclusions are spheroidal; the resulting matrices are transversely isotropic in the x–y plane and do not change under arbitrary rotation about the z axis.

The similarly oriented and 3D random NRP effective moduli described above are for 2 phase composites, which is sufficient for the purposes of investigating the effect of waviness on NRP modulus in this article. In an actual NRP, however, the NTs will likely have different waviness characteristics (λ/d, a/λ) and perhaps different moduli as well (E_{NT}/E_M). Such a system can also be analyzed using Weng's approach [21] by discretizing the distribution of parameters (λ/d, a/λ, E_{NT}/E_M) into individual phases. The effective modulus is then obtained by considering the material as a multiphase composite using Eq. (5), where the strain concentration matrix $\mathbf{A}\left(=\mathbf{A}^{r,\mathrm{dil}}\right)$ is determined for each of the $N-1$ inclusion phases utilizing the finite element solution approach described above.

3.4. Analytical long wavelength model

Although the finite element model approach developed to this point is quite powerful, it would be preferable to have an analytical model to calculate the strain concentration matrix. The analytical long wavelength (ALW) model developed below allows such an analytical approach for a nanotube with a very large wavelength ratio λ/d. Consider an infinitesimal slice of the sinusoidal NT embedded in an infinite matrix as shown in Fig. 4. The central hypothesis of the ALW model is that as the NT wavelength λ becomes very large with respect to its diameter d, the average strain in this NT section approaches that of an infinitely long straight NT oriented at the same angle α and embedded in an infinite matrix. If this is the case, the average strain $\langle\varepsilon^{uvw}\rangle^{dz}$ in the slice dz in the local coordinate system (uvw) is given by

$$\langle\varepsilon^{uvw}\rangle^{dz} = \hat{\mathbf{A}}\,\tilde{\varepsilon}^{uvw} \tag{19}$$

where $\tilde{\varepsilon}^{uvw}$ is the applied farfield strain rotated to the uvw coordinate system and $\hat{\mathbf{A}}$ is the strain concentration matrix for an infinitely long straight fiber developed using Eshelby's equivalent inclusion method (see companion article [15] for details in calculating $\hat{\mathbf{A}}$). All terms above reflect the reduced 6×6 matrix notation [for example, see Eq. (13)]. For simplicity, assume that the strain vectors in Eq. (19) consist of tensorial strains; a similar derivation using engineering shear strains yields identical results.

The transformation matrix $\mathbf{T}$ to rotate strains from the global xyz coordinate system to local uvw coordinate system is easily derived using tensor transformation laws. When converted to the matrix form, this relationship becomes

$$\varepsilon^{uvw} = \mathbf{T}(\alpha)\,\varepsilon^{xyz}$$

$$\begin{Bmatrix} \varepsilon_{11}^{uvw} \\ \varepsilon_{22}^{uvw} \\ \varepsilon_{33}^{uvw} \\ \varepsilon_{23}^{uvw} \\ \varepsilon_{13}^{uvw} \\ \varepsilon_{12}^{uvw} \end{Bmatrix} =$$

$$\begin{bmatrix} 1 & 0 & 0 & 0 & 0 & 0 \\ 0 & \cos^2\alpha & \sin^2\alpha & 2p\sin\alpha\cos\alpha & 0 & 0 \\ 0 & \sin^2\alpha & \cos^2\alpha & -2p\sin\alpha\cos\alpha & 0 & 0 \\ 0 & -p\sin\alpha\cos\alpha & p\sin\alpha\cos\alpha & \cos^2\alpha - \sin^2\alpha & 0 & 0 \\ 0 & 0 & 0 & 0 & \cos\alpha & p\sin\alpha \\ 0 & 0 & 0 & 0 & -p\sin\alpha & \cos\alpha \end{bmatrix}$$

$$\times \begin{Bmatrix} \varepsilon_{11}^{xyz} \\ \varepsilon_{22}^{xyz} \\ \varepsilon_{33}^{xyz} \\ \varepsilon_{23}^{xyz} \\ \varepsilon_{13}^{xyz} \\ \varepsilon_{12}^{xyz} \end{Bmatrix} \tag{20}$$

where $\mathbf{T}(\alpha)$ is the transformation matrix for the angle α (see Fig. 4) and the constant p is defined as 1. The matrix $\mathbf{T}^{-1}(\alpha)$ is defined as the transformation from the uvw coordinate system to 123 coordinate system; it is identical to $\mathbf{T}(\alpha)$ above except with $p = -1$. Substituting

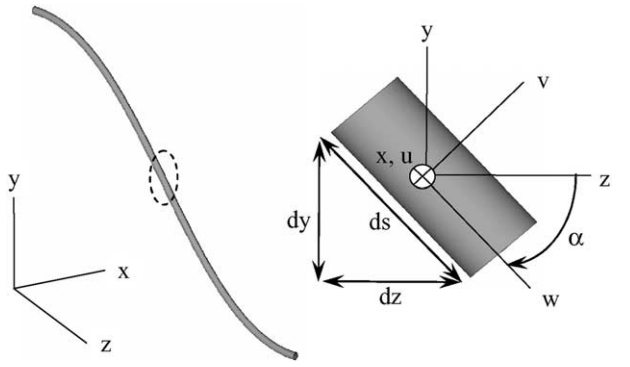

Fig. 4. Small section of sinusoidal NT embedded in an infinite matrix (global axis system *xyz*, local axis system *uvw*).

the transformation in Eq. (20) for both strain terms in Eq. (19) and rearranging leads to the relationship

$$\langle \varepsilon^{123} \rangle^{dz} = \mathbf{T}^{-1}(\alpha)\,\hat{\mathbf{A}}\,\mathbf{T}(\alpha)\,\tilde{\varepsilon}^{123} \tag{21}$$

The average volumetric strain for the entire NT is then obtained by integrating this expression over a single NT wavelength. The angle α at any point along the NT can be obtained by differentiating Eq. (6) to find

$$\alpha(z) = \tan^{-1}\left[-\frac{2\pi a}{\lambda}\sin\left(\frac{2\pi z}{\lambda}\right)\right] \tag{22}$$

The volume occupied by the infinitesimal slice of NT is given by

$$\mathrm{d}V = \frac{\pi \mathrm{d}^2}{4}\,\mathrm{d}s = \frac{\pi \mathrm{d}^2}{4}\frac{\mathrm{d}z}{\cos\alpha(z)} \tag{23}$$

Thus, the average strain in the entire NT is given by

$$\langle \varepsilon \rangle = \frac{\int_V \langle \varepsilon^{123} \rangle^{dz}\,\mathrm{d}V}{\int_V \mathrm{d}V} = \frac{\int_0^L \dfrac{\mathbf{T}^{-1}[\alpha(z)]\,\hat{\mathbf{A}}\,\mathbf{T}[\alpha(z)]\,\tilde{\varepsilon}^{123}}{\cos\alpha(z)}\,\mathrm{d}z}{\int_0^L \dfrac{\mathrm{d}z}{\cos\alpha(z)}} \tag{24}$$

Since $\tilde{\varepsilon}^{123}$ is the constant farfield strain, it can be pulled outside of the integral. The final ALW expression for the strain concentration matrix $\mathbf{A}^{\mathrm{ALW}}$ is thus obtained as

$$\mathbf{A}^{\mathrm{ALW}} = \frac{\int_0^L \dfrac{\mathbf{T}^{-1}[\alpha(z)]\,\hat{\mathbf{A}}\,\mathbf{T}[\alpha(z)]}{\cos\alpha(z)}\,\mathrm{d}z}{\int_0^L \dfrac{\mathrm{d}z}{\cos\alpha(z)}} \tag{25}$$

This expression must be solved numerically. The resulting strain concentration matrix has the same form as Eq. (13). It will be demonstrated in the results section that the strain concentration matrix from the finite element model does indeed approach the ALW model with as the wavelength ratio λ/d becomes large.

4. Results

This section utilizes the relationships developed in the previous two sections to predict the effective stiffness of NRPs consisting of wavy NTs via the NSCT model. Specifically, NRPs with 2 phases are studied (i.e. $N=2$), which consist of a single type of nanotube inclusion (with all NTs having common stiffness and waviness properties λ/d, a/λ and $E_{\mathrm{NT}}/E_{\mathrm{M}}$) embedded in a matrix phase. Analysis of an NRP consisting of several nanotube inclusion phases can also be performed ($N > 2$); see the companion article for such a presentation [15].

This section begins with an analysis of the terms of the strain concentration matrix obtained from the finite element model. Then, a composite where all wavy NTs have a similar orientation is considered; the results will be compared to the effective reinforcing modulus model in the companion paper as well as the ALW model. Finally, a composite consisting of randomly oriented NTs with identical properties (λ/d, a/λ, $E_{\mathrm{NT}}/E_{\mathrm{M}}$) is examined. It will be demonstrated that for such a composite, the ALW model predicts properties identical to a composite consisting of randomly oriented, infinitely long straight NTs. Furthermore, it will be shown that as λ/d increases, the prediction using the finite element model case approaches the ALW model as initially hypothesized. The implications of this finding for wavy NT composites will be discussed.

4.1. Strain concentration matrix terms

The strain concentration matrix was obtained for the following cases:

- modulus ratio $E_{\mathrm{NT}}/E_{\mathrm{M}}$ (2 values): 200, 400
- wavelength ratio λ/d (12 values): 10, 17.78, 31.62, 56.23, 100, 177.8, 316.2, 562.3, 749.9, 1000, 1334, 1778
- waviness ratio a/λ (11 values): 0, 0.01, 0.01778, 0.03162, 0.05623, 0.10, 0.1334, 0.1778, 0.2371, 0.3162, 0.4217

For each combination (264 total), the 12 independent terms of the strain concentration matrix were determined [see Eq. (13)]. The values for λ/d and a/λ are spaced logarithmically with the exception of $a/\lambda=0$; this is the straight NT case and it was verified to give identical results as the Eshelby dilute solution strain concentration matrix.

As a starting point, consider the two strain concentration matrices shown in Fig. 5. The first case (a) is from the Eshelby solution for straight fibers ($a/\lambda=0$);

$$\begin{bmatrix} 0.0037 & -0.0002 & -0.2990 & 0 & 0 & 0 \\ -0.0002 & 0.0037 & -0.2990 & 0 & 0 & 0 \\ 0 & 0 & 1 & 0 & 0 & 0 \\ 0 & 0 & 0 & 0.0050 & 0 & 0 \\ 0 & 0 & 0 & 0 & 0.0050 & 0 \\ 0 & 0 & 0 & 0 & 0 & 0.0039 \end{bmatrix}$$

(a) $a/\lambda = 0$

;

$$\begin{bmatrix} 0.0037 & -0.1112 & -0.1093 & 0 & 0 & 0 \\ -0.0001 & 0.1516 & 0.1164 & 0 & 0 & 0 \\ -0.0001 & 0.1136 & 0.1418 & 0 & 0 & 0 \\ 0 & 0 & 0 & 0.2713 & 0 & 0 \\ 0 & 0 & 0 & 0 & 0.0045 & 0 \\ 0 & 0 & 0 & 0 & 0 & 0.0045 \end{bmatrix}$$

(b) $a/\lambda = 0.3162$

Fig. 5. Two strain concentration matrix solutions with $\lambda/d = 100$ and ratio $E_{NT}/E_M = 400$ (a) $a/\lambda = 0$ and (b) $a/\lambda = 0.3162$; similar values highlighted in the text are italicized.

see the companion article [15] for the equations to calculate the Eshelby strain concentration matrix. The second is from the finite element method run for moderate waviness ($a/\lambda = 0.3162$). Several items are of interest. First, the terms A_{11}, A_{21}, A_{31}, A_{55} and A_{66} are small and virtually identical in both cases; these have been highlighted with italics. As these terms relate to far field strains in the x direction (strains $\tilde{\varepsilon}_{11}$, $\tilde{\varepsilon}_{13}$, $\tilde{\varepsilon}_{12}$), this indicates that the NT response to strains normal to the plane of waviness (y–z) is affected little by NT waviness. By comparison, the remaining seven terms that are related to loading in the waviness plane ($\tilde{\varepsilon}_{22}$, $\tilde{\varepsilon}_{33}$ $\tilde{\varepsilon}_{23}$) are affected dramatically. Of greatest interest is A_{33}, which relates the NT strain in the 3 direction to an applied farfield strain in the same direction. For a straight NT composite, this is the key reinforcement term. With the introduction of significant waviness, this value has decreased by a factor of seven indicating a significant reduction in stiffness in the 3 direction relative to the straight NT case.

While it is useful to consider the entire strain concentration matrix as in Fig. 5, it is easier to visualize the effect of the variables by plotting a single term; A_{33} is chosen for this case and the results are shown in Fig. 6. The prediction from the ALW model is also shown. Recall that the ALW model was developed with the idea that it would apply to wavy NT composites with long wavelength. Fig. 6 validates this hypothesis, as the independently developed finite element model results do indeed tend to the ALW model as λ/d increases. The

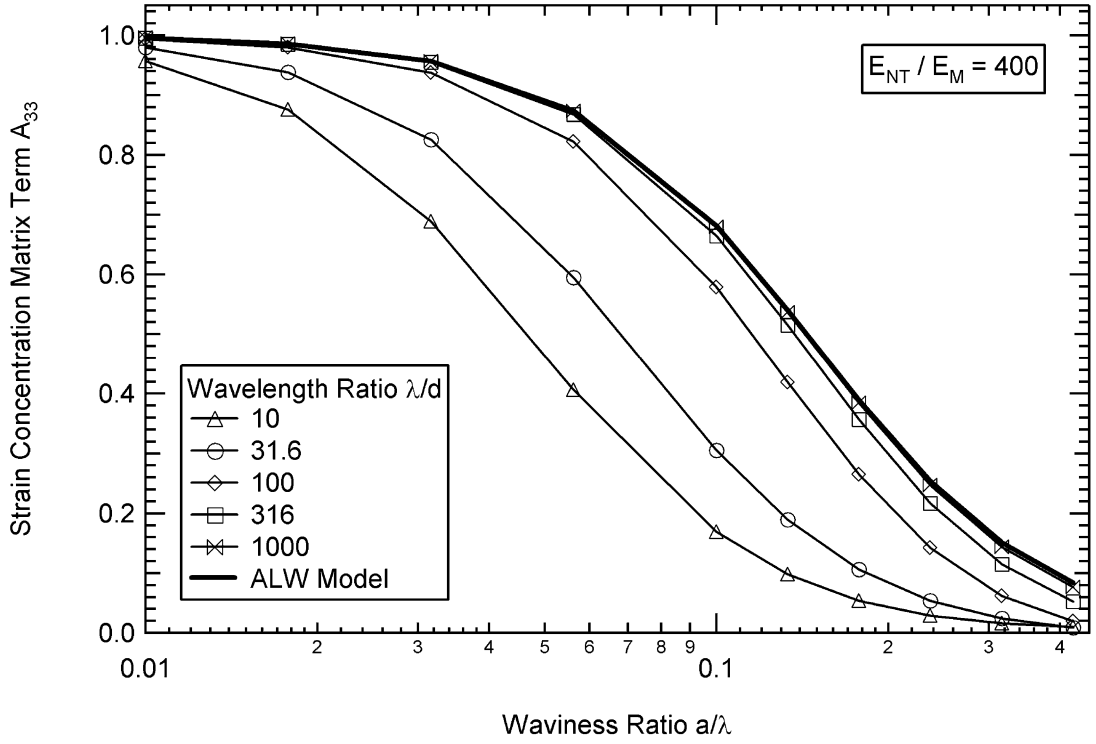

Fig. 6. Strain concentration matrix term A_{33} versus a/λ for the finite element model with various λ/d values and analytical long wavelength (ALW) model.

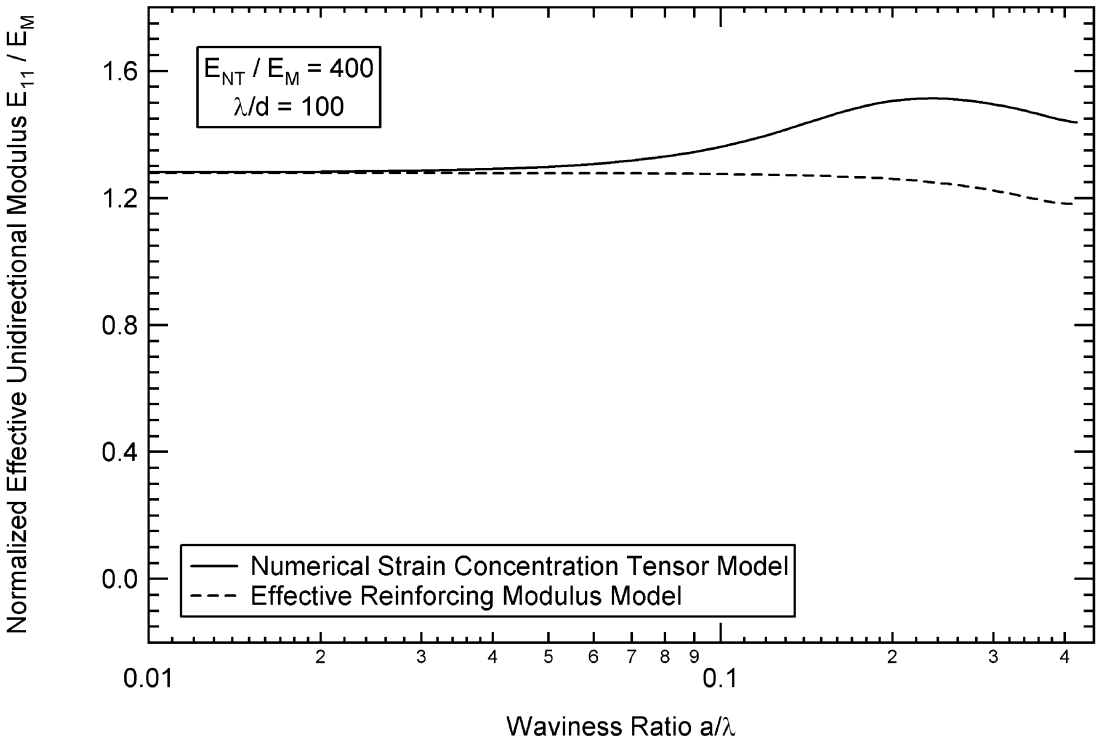

Fig. 7. Variation of the modulus term E_{11} (in the x direction of Fig. 1) with increasing waviness ratio (a/λ) for the ERM and NSCT models.

result for λ/d of 1000 is virtually identical to the ALW model result. It should be noted that this finding is not due to a "flattening out" of the wavy NTs for increasing λ/d (i.e. waviness amplitude $a << \lambda$ so it appears to be a nearly straight NT) since the independent axis is also a ratio of the two (a/λ).

4.2. Similarly oriented NRP modulus

This section considers a composite with similarly oriented inclusions (common E_{NT}/E_M, λ/d, a/λ), all aligned with the global axis as in Figs. 1 and 3a. The effective modulus **C*** was calculated using the Mori–Tanaka theory via Eq. (5). The NT volume fraction f_1 was taken to be 10%. From the effective modulus **C***, the resulting orthotropic engineering properties of the composite (E_{11}, E_{22}, E_{33}, ν_{12}, ν_{13}, ν_{23}, G_{12}, G_{13} and G_{23}) can be determined[24] The modulus terms were compared to those from the effective reinforcing modulus model developed in the companion paper [15]; the results for the modulus terms E_{11}, E_{22} and E_{33} are shown in Figs. 7, 8 and 9, respectively, for a wavelength ratio (λ/d) of 100 as a function of waviness ratio (a/λ).

One surprising result is the difference in the E_{33} term (Fig. 9) between the NSCT and ERM models; since the effective reinforcing modulus in the companion paper is based on a finite element model modulus result in the 3 direction, one might expect that both models would have nearly identical E_{33} results. At low volume fractions (0.1% and lower), this is indeed the case.[8] The reason for the difference as the volume fraction increases is that the inclusion interaction provided for by the Mori–Tanaka theory is more accurately modeled in the NSCT approach. The effective reinforcing modulus model considers the wavy NTs as straight inclusions with a reduced modulus; the modulus in the inclusion (NT) direction for such materials is nearly identical when obtained using the Mori–Tanaka theory (inclusion interaction) or a simple rule of mixtures (no inclusion interaction). Thus, inclusion interaction plays a small role in the fiber-direction modulus for an NRP with straight NTs. For the NSCT model, however, interaction between the wavy NTs affects the reinforcement provided, resulting in a lower E_{33} modulus when compared to the ERM model.

The E_{11} term (Fig. 7) shows little variation with waviness ratio (a/λ), with the two models leading to

[8] This finding points out an interesting feature of the model developed in this paper. Once the strain concentration matrix **A** is known for a single wavy NT embedded in an infinite matrix (obtained via analysis of the model in Fig. 1a), the Mori–Tanaka theory can be used to predict the modulus E_{cell} (E_{33}) of the cell shown in Fig. 1(b); this leads [via Eq. (15)] to the effective reinforcing modulus (E_{ERM}) that is the basis of the companion paper. Thus, it is not necessary to complete a separate finite element solution to determine the effective fiber modulus if the strain concentration matrix **A** is already known. As pointed out in the text, the NT volume fraction used in such an evaluation ($f_1 = f_{cell}$) should be set to an appropriately small value to satisfy the dilute approximation (for example, 0.01% or lower).

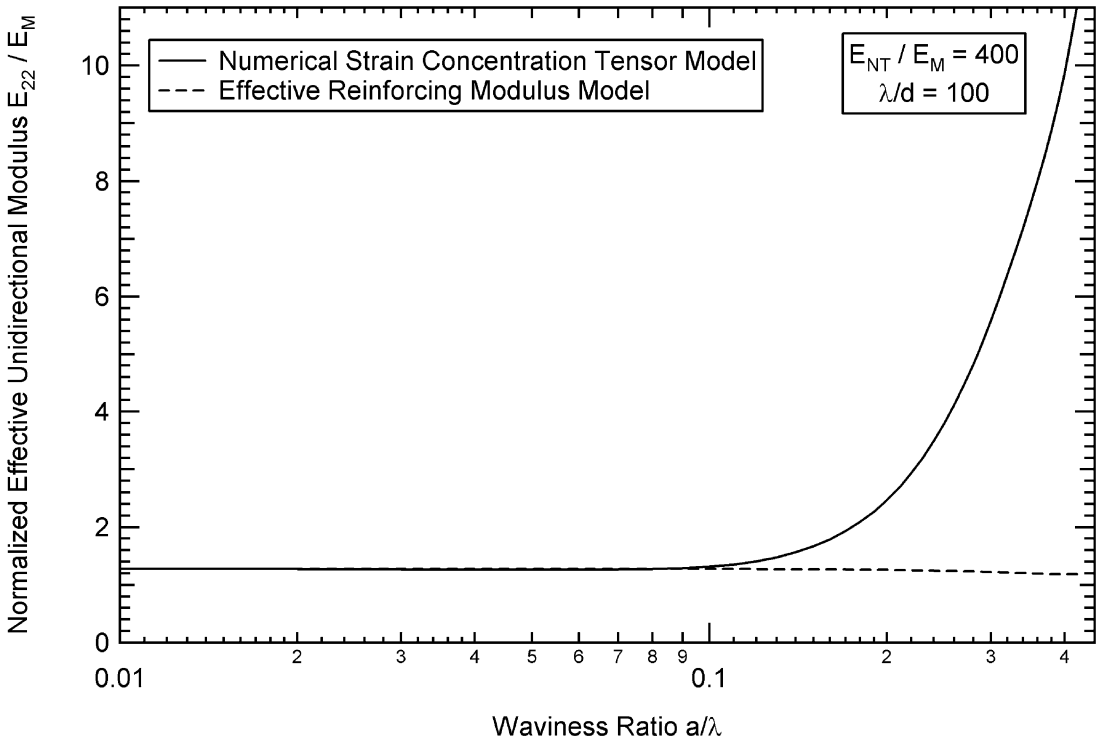

Fig. 8. Variation of the modulus term E_{22} (in the y direction of Fig. 1) with increasing waviness ratio (a/λ) for the ERM and NSCT models.

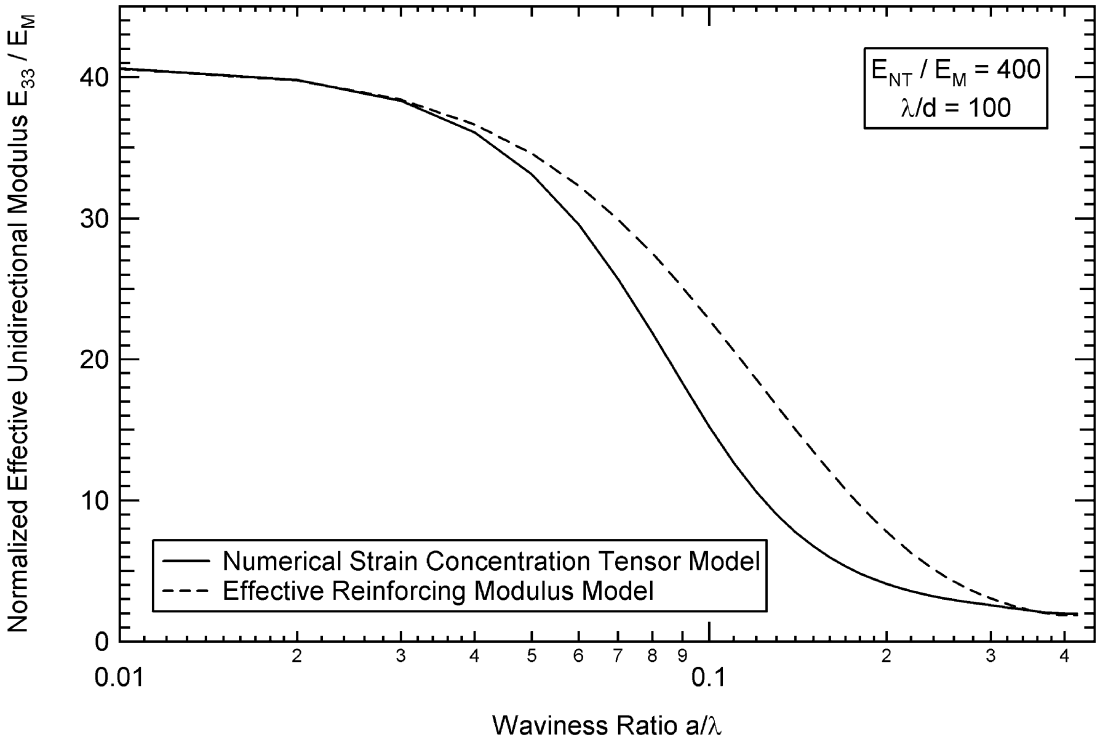

Fig. 9. Variation of the modulus term E_{33} (in the z direction of Fig. 1) with increasing waviness ratio (a/λ) for the ERM and NSCT models.

somewhat different results; this is consistent with the earlier finding for the strain concentration matrix in Fig. 5 that showed waviness has little effect for loading in the direction normal to the plane of waviness. However, the E_{22} term is strikingly different for the two models as shown in Fig. 8. This is explained by recalling that the ERM model considers the wavy NT composite as a straight NT composite with waviness effects accounted for by an effective (reduced) NT modulus. This results in a material that is transversely isotropic in the $x-y$ plane ($E_{11}=E_{22}$). Furthermore, since the effective reinforcing modulus decreases with increased waviness ratio (a/λ), the associated model predicts E_{22} also decreases with increasing a/λ. Consideration of the geometry, however, makes it clear that this result is not correct; as the waviness ratio (a/λ) increases, the NT begins to reinforce the material in the 2 direction, causing an increase in E_{22}. Indeed, in the limit case when the waviness ratio a/λ goes to infinity, the wavy NTs approach straight NTs with their axis in the 2 direction; this leads to a significant modulus increase relative to the matrix material. This difference in E_{22} for the two models will have ramifications in modulus predictions for randomly oriented wavy NT composites.

4.3. Randomly oriented wavy NRP modulus

The strain concentration matrix determined from the finite element solution presented in the previous section is used to predict the modulus $\mathbf{C}^*$ for a composite consisting of randomly oriented wavy NTs (Fig. 3b) using Eq. (5). For the ERM model, Eq. (5) is also used with $\mathbf{C}^{\mathrm{r}}$ calculated using the effective reinforcing modulus E_{ERM} obtained from Eq. (15) and $\mathbf{A}^{r,\,\mathrm{dil}}$ is determined for a straight NT using Eshelby's solution. Once the modulus $\mathbf{C}^*$ is known for the randomly oriented composite, calculation of the isotropic Young's modulus E and Poisson's ratio v is straightforward.

The Young's modulus results for the two models with $\lambda/d=10$ and 100 are shown in Fig. 10. For the short wavelength case ($\lambda/d=10$), the results are fairly similar. For the longer wavelength case ($\lambda/d=100$), the NSCT method predicts a stiffer composite response than the ERM model, especially for waviness ratios $a/\lambda > 0.10$. This difference is due to the stiffer response in the 2 direction predicted by the current model for a similarly oriented NT composite (see Fig. 8), which results in an increased stiffness, relative to the ERM model, when the NTs are randomly oriented in the composite. It should also be noted that the NSCT modulus in Fig. 10 initially decreases and then increases as a/λ increases. As a/λ becomes large, the fibers begin to appear straight in the 2 direction (see the earlier discussion regarding Fig. 8). Thus, in the asymptotic case of $a/\lambda \to \infty$, the modulus of the randomly oriented composite must approach that for the composite with randomly oriented straight fibers ($a/\lambda=0$). This causes the increase in modulus seen in Fig. 10 once a/λ becomes sufficiently large.

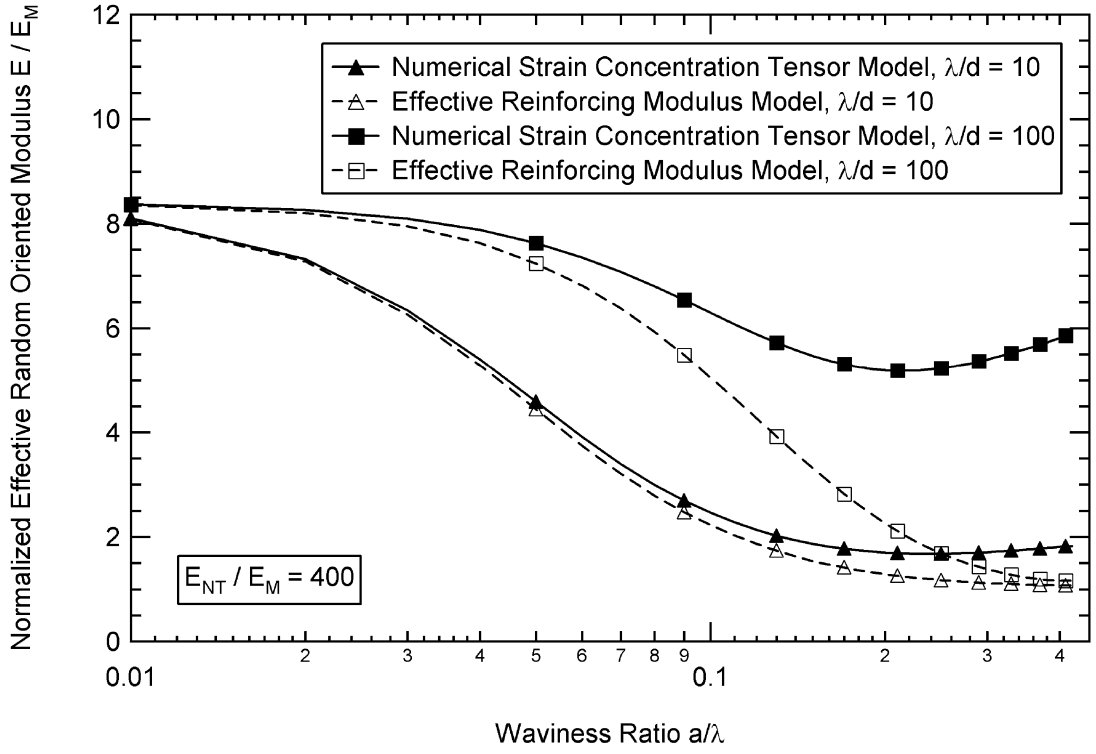

Fig. 10. Variation of the Young's modulus for an NRP with randomly oriented wavy NTs.

The modulus of elasticity result for the NSCT model is shown for increasing values of λ/d in Fig. 11. Also shown is the prediction from the ALW model (derived for large λ/d), which is nearly constant. The reason that the ALW model result is independent of the waviness ratio a/λ is easily explained. The hypothesis behind the ALW model is that each segment of the sinusoidal NT acts as though it is part of an infinitely long straight NT with an identical orientation. Once these wavy NTs are randomly oriented, each of these segments (with the character of straight NTs) become randomly oriented as well; thus, the overall behavior of the randomly oriented wavy NT composite in the ALW model is equivalent to that of a composite consisting of randomly oriented straight NTs regardless of the waviness ratio a/λ.

As with the similarly oriented wavy NT composite result, the randomly oriented wavy NT composite modulus from the current model approaches the ALW model as λ/d increases. Therefore, if the NTs are randomly oriented and the wavelengths λ are sufficiently large relative to the NT diameter d, the effect of waviness is likely to be minimal and the elastic material behavior is the same as for an NRP with randomly oriented straight NTs.

4.4. Modulus predictions for actual NRPs

For many NRPs, the randomly oriented NTs will be wavy but with wavelengths such that the ALW model does not apply. The effect that waviness plays in the modulus of such materials can be assessed using the numerical strain concentration tensor model developed in this paper. The first step is to perform a survey of the NT geometry to understand the nature of the NT waviness; this will take the form of a distribution of NTs with various values of a/λ, λ/d and perhaps E_{NT}/E_M. Once this distribution is determined, the NRP can be modeled as a multiphase composite using Eq. (5) with the strain concentration tensor for each phase determined using the finite element approach detailed in this paper.

The companion article [15] performed a preliminary assessment of waviness for several NTs using a transmission electron microscope image reported by other researchers[11]. For this single figure, the waviness ratio a/λ ranged from 0 to 0.25 (most at 0.10 or less) while the wavelength ratio λ/d ranged from 25 to 150. More thorough assessments of this nature should be performed to predict the effect of waviness in an actual NRP. Although the NSCT model developed in this paper and the ERM model developed in the companion paper lead to strikingly different predictions for randomly oriented composites (see Fig. 10), the differences are fairly small for waviness ratios a/λ in the range of 0–0.10 with wavelength ratios λ/d in the range of 10–100. Thus, for moderately wavy NTs, either model should give sufficiently accurate results. Beyond this range, the NSCT model is preferable.

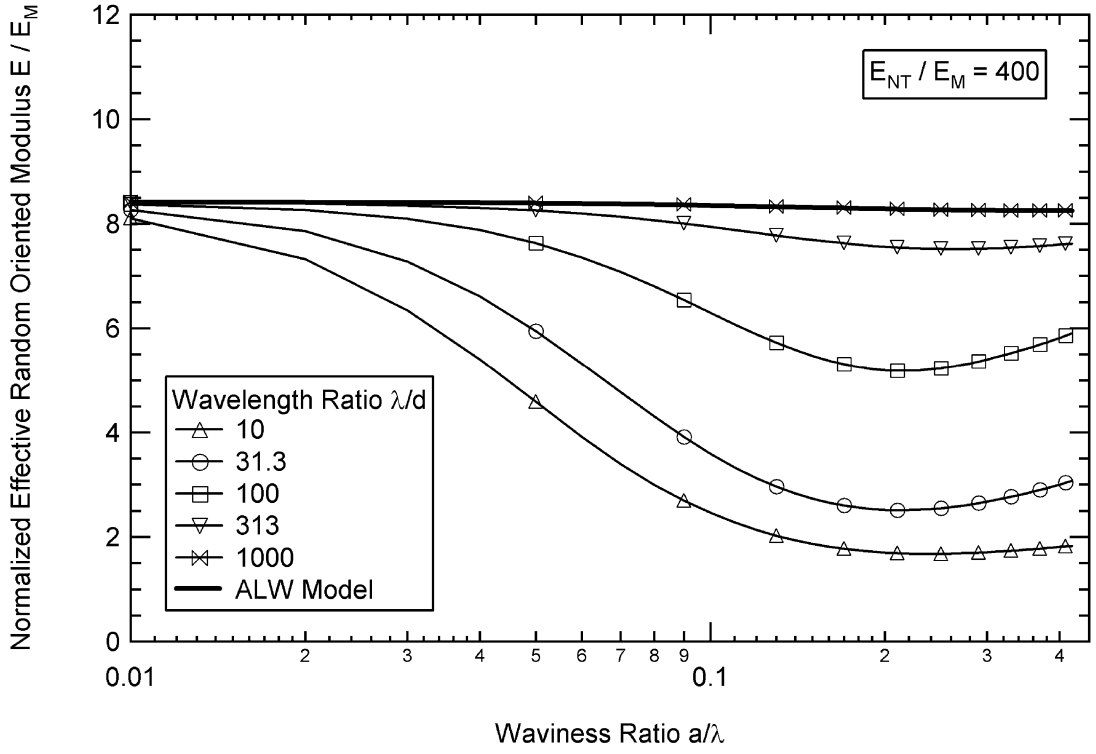

Fig. 11. Variation of the Young's modulus for an NRP with randomly oriented wavy NTs calculated using the NSCT model for various λ/d values.

5. Conclusions

Polymer systems reinforced with carbon nanotubes offer potential benefits over traditional reinforcement methods in terms of mechanical, electrical and thermal behavior. The degree of improvement for mechanical stiffness (modulus) is dictated by a variety of factors, including nanotube properties, bonding between the nanotube and the matrix and nanotube dispersion in the matrix. One factor that has received little attention to date is the impact that nanotube waviness plays once the nanotubes are embedded in the polymer. While one expects non-straight NTs to perform less well as a reinforcing phase compared to straight NTs, the degree of the difference has been unclear.

This article addresses this question by developing a model that is a hybrid of finite element modeling and classical micromechanics techniques. This model considers the wavy nanotube as an infinitely long sinusoid perfectly embedded in the matrix material. The response of this system is a function of three governing parameters: the sinusoidal wavelength-to-diameter ratio λ/d, the sinusoidal amplitude-to-wavelength ratio a/λ and the ratio of the nanotube and polymer moduli E_{NT}/E_M. The model demonstrates that waviness will indeed reduce the modulus in the nanotube direction of a polymer reinforced with similarly oriented wavy nanotubes when compared to a similar material consisting of only straight nanotubes. However, when the wavy nanotubes are randomly oriented in the polymer, the degree of modulus reduction varies from significant to minimal, depending on the sinusoidal wavelength ratio λ/d. As this ratio increases to large values, each wavy nanotube begins to act as a collection of infinitely long straight nanotube segments. This result agrees with the analytical long wavelength model presented here, which is applicable when λ/d becomes sufficiently large.

The novel finite element-micromechanics approach used in this paper can be used to study other non-ellipsoidal inclusion geometries. Future work will utilize this feature to consider various items of interest including anisotropic nanotube material properties, investigation of effect of hollow nanotube representations, and the impact of finite nanotube lengths. However, it should be noted that this model and its results are based on the idea that continuum mechanics can provide insight into the behavior of nanoscale systems, which is a first approximation of the actual system. Future work will also consider atomic scale models to assess many of these same questions regarding the nature of the nanotube embedded in a polymer matrix. In the matrix material away from the nanotube, traditional continuum mechanics will again apply and a hybrid atomic-continuum approach can be developed.

Acknowledgements

The authors would like to acknowledge the support for this work provided by the NASA Langley Computational Materials Nanotechnology Program.

References

[1] Callister Jr WD. Materials science and engineering: an introduction, 4th ed. New York: John Wiley & Sons, Inc; 1997.
[2] Toray Carbon Fibers America, I. Toray tecnical manual. Santa Ana, CA: 2000.
[3] Che J, Çagin T, Goddard III W. Generalized extended empirical bond-order dependent force fields including nonbond interactions. Theoretical Chemistry Accounts 1999;102:346–54.
[4] Gao G, Çagin T, Goddard III WA. Energetics, structure, mechanical and vibrational properties of single-walled carbon nanotubes. Nanotechnology 1998;9:184.
[5] Hernández E, et al. Elastic properties of C and $B_xC_yN_z$ composite nanotubes. Physical Review Letters 1998;80(20):4502.
[6] Sánchez-Portal S, et al. Ab initio structural, elastic, and vibrational properties of carbon nanotubes. Physical Review B 1999; 59(19):12678.
[7] Salvetat J-P, et al. Mechanical properties of carbon nanotubes. Applied Physics A 1999;69:255–60.
[8] Belytschko T, et al. Atomistic simulations of nanotube fracture. Physics Review B [in press].
[9] Sandler J, et al. Development of a dispersion process for carbon nanotubes in an epoxy matrix and the resulting electrical properties. Polymer 1999;40(21):5967.
[10] Andrews R, et al. Processing of nanotube-polymer composites by shear mixing. Macromolecular Materials and Engineering [in press].
[11] Qian D, et al. Load transfer and deformation mechanisms in carbon nanotube-polystyrene composites. Applied Physics Letters 2000;76(20):2868.
[12] Schadler LS, Giannaris SC, Ajayan PM. Load transfer in carbon nanotube epoxy composites. Applied Physics Letters 1998;73(26): 3842.
[13] Fisher FT, Bradshaw RD, Brinson LC. Effects of nanotube waviness on the modulus of nanotube-reinforced polymers. Applied Physics Letters 2002;80(24):4647–9.
[14] Shaffer MSP, Windle AH. Fabrication and characterization of carbon nanotube/poly(vinyl alcohol) composites. Advanced Materials 1999;11(11):937.
[15] Fisher FT, Bradshaw RD, Brinson LC. Fiber waviness in nanotube-reinforced polymer composites: I. Modulus predictions using effective nanotube properties. Composites Science and Technology [in press].
[16] Aboudi J. Mechanics of composite materials: a unified micromechanics approach. Studies in Applied Mechanics, vol. 29. Amsterdam: Elsevier; 1991.
[17] Chou T-W, Takahashi K. Non-linear elastic behaviour of flexible fibre composites. Composites 1987;18(1):25–34.
[18] Kuo C-M, Takahashi K, Chou T-W. Effect of fiber waviness on the nonlinear elastic behavior of flexible composites. Journal of Composite Materials 1988;22:1004–25.
[19] Tandon GP, Weng GJ. Average stress in the matrix and effective moduli of randomly orientated composites. Composites Science and Technology 1986;27:111–32.
[20] Huang JH. Some closed-form solutions for effective moduli of composites containing randomly oriented short fibers. Materials Science and Engineering A 2001;315:11–20.
[21] Weng GJ. The theoretical connection between Mori–Tanaka's

theory and the Hashin-Shtrikman-Wadpole bounds. International Journal of Engineering Science 1990;28(11):1111–20.
[22] Fisher, F.T., Nanomechanics of carbon nanotube-reinforced polymers. PhD thesis, Northwestern University, Department of Mechanical Engineering; 2002.
[23] Malvern LE. Introduction to the mechanics of a continuous medium. In: Reswick JB, Rohsenow WM, editors. Engineering of the physical sciences. Englewood Cliffs, NJ: Prentice-Hall Inc; 1969.
[24] Jones RM. Mechanics of composite materials. New York, NY: Hemisphere Publishing Corporation; 1975.